

An Effective Model of the Retinoic Acid Induced HL-60 Differentiation Program

Ryan Tasseff, Holly A. Jensen, Wei Dai, Katherine Rogers, Adithya Sagar, Rodica P. Bunaciu[†], Johanna Congleton[†], Andrew Yen[†], and Jeffrey D. Varner*

Robert Frederick Smith School of Chemical and Biomolecular Engineering and [†]Department of Biomedical Sciences, Cornell University, Ithaca NY 14853

Running Title: Effective modeling of HL-60 differentiation

To be submitted: *Frontiers in Systems Biology*

*Corresponding author:

Jeffrey D. Varner,

Professor, Robert Frederick Smith School of Chemical and Biomolecular Engineering,
244 Olin Hall, Cornell University, Ithaca NY, 14853

Email: jdv27@cornell.edu

Phone: (607) 255 - 4258

Fax: (607) 255 - 9166

Abstract

In this study, we present an effective model All-Trans Retinoic Acid (ATRA)-induced differentiation of HL-60 cells. The model describes a key architectural feature of ATRA-induced differentiation, positive feedback between an ATRA-inducible signalsome complex involving many proteins including Vav1, a guanine nucleotide exchange factor, and the activation of the mitogen activated protein kinase (MAPK) cascade. The model, which was developed by integrating logical rules with kinetic modeling, was significantly smaller than previous models. However, despite its simplicity, it captured key features of ATRA induced differentiation of HL-60 cells. We identified an ensemble of effective model parameters using measurements taken from ATRA-induced HL-60 cells. Using these parameters, model analysis predicted that MAPK activation was bistable as a function of ATRA exposure. Conformational experiments supported ATRA-induced bistability. These findings, combined with other literature evidence, suggest that positive feedback is central to a diversity of cell fate programs.

1 Introduction

2 Understanding the architecture of differentiation programs is an important therapeutic
3 challenge. Differentiation induction chemotherapy (DIC), using agents such as the vita-
4 min A derivative all-trans retinoic acid (ATRA), is a promising approach for the treatment
5 of many cancers (1–3). For example, ATRA treatment induces remission in 80–90% of
6 promyelocytic leukemia (APL) PML-RAR α -positive patients (4), thereby transforming a
7 fatal diagnosis into a manageable disease. However, remission is sometimes not durable
8 and relapsed cases exhibit emergent ATRA resistance (5, 6). To understand the basis of
9 this resistance, we must first understand the ATRA-induced differentiation program. To-
10 ward this challenge, lessons learned in model systems, such as the lineage-uncommitted
11 human myeloblastic cell line HL-60, could inform our analysis of the more complex dif-
12 ferentiation programs occurring in patients. Patient derived HL-60 leukemia cells have
13 been a durable experimental model since the 1970's to study differentiation (7). HL-60
14 undergoes cell cycle arrest and either myeloid or monocytic differentiation following stim-
15 ulation; ATRA induces G1/G0-arrest and myeloid differentiation in HL-60 cells, while 1,25-
16 dihydroxy vitamin D3 (D3) induces arrest and monocytic differentiation. Commitment to
17 cell cycle arrest and differentiation requires approximately 48 hr of treatment, during which
18 HL-60 cells undergo two division cycles.

19 Sustained mitogen-activated protein kinase (MAPK) activation is a defining feature of
20 ATRA-induced HL-60 differentiation. ATRA drives sustained MEK-dependent activation
21 of the Raf/MEK/ERK pathway, leading to arrest and differentiation (8). MEK inhibition re-
22 sults in the loss of ERK and Raf phosphorylation, and the failure to arrest and differentiate
23 (9). ATRA (and its metabolites) are ligands for the hormone activated nuclear transcrip-
24 tion factors retinoic acid receptor (RAR) and retinoid X receptor (RXR) (10). RAR/RXR
25 activation is necessary for ATRA-induced Raf phosphorylation (9), and the formation of
26 an ATRA-inducible signalsome complex at the membrane which drives MAPK activation

27 through a yet to be identified kinase activity. While the makeup of the signalsome com-
28 plex is not yet known, we do know that it is composed of Src family kinases Fgr and Lyn,
29 PI3K, c-Cbl, Slp76, and KSR, as well as IRF-1 transcription factors (11–15). Signalsome
30 formation and activity is driven by ATRA-induced expression of CD38 and the putative
31 heterotrimeric Gq protein-coupled receptor BLR1 (16, 17). BLR1, identified as an early
32 ATRA (or D3)-inducible gene using differential display (18), is necessary for MAPK ac-
33 tivation and differentiation (17), and is also involved with signalsome activity. Studies
34 of the BLR1 promoter identified a 5' 17bp GT box approximately 1 kb upstream of the
35 transcriptional start that conferred ATRA responsiveness (17). Members of the BLR1
36 transcriptional activator complex, e.g. NFATc3 and CREB, are phosphorylated by ERK,
37 JNK or p38 MAPK family members suggesting positive feedback between the signal-
38 some and MAPK activation (19). BLR1 overexpression enhanced Raf phosphorylation
39 and accelerated terminal differentiation, while Raf inhibition reduced BLR1 expression
40 and differentiation (20). BLR1 knock-out cells failed to activate Raf or differentiate in
41 the presence of ATRA (20). Interestingly, both the knockdown or inhibition of Raf, also
42 reduced BLR1 expression and functional differentiation (20). Thus, the expression of
43 signalsome components e.g., BLR1 was Raf dependent, while Raf activation depended
44 upon the siganlsome. A recent computational study of ATRA-induced differentiation in
45 HL-60 cells suggested that the BLR1-MAPK positive feedback circuit was sufficient to ex-
46 plain ATRA-induced sustained MAPK activation, and the expression of a limited number
47 of functional differentiation markers (21). Model analysis also suggested that Raf was the
48 most distinct of the MAPK proteins. However, this previous study developed and analyzed
49 a complex model, thus leaving open the critical question of what is the minimal positive
50 feedback circuit required to drive ATRA-induced differentiation.

51 In this study, we explored this question using a minimal mathematical model of the
52 key architectural feature of ATRA induced differentiation of HL-60 cells, namely positive

53 feedback between an ATRA-inducible signalsome complex and MAPK activation. The
54 ATRA responsive signalsome-MAPK circuit was then used to drive a downstream gene
55 expression program which encoded for the expression of functional differentiation mark-
56 ers. The effective model used a novel framework which integrated logical rules with ki-
57 netic modeling to describe gene expression and protein regulation, while largely relying
58 upon biophysical parameters from the literature. This formulation significantly reduced
59 the size and complexity of the model compared to the previous study of Tasseff et al.,
60 while increasing the breadth of the biology described (21). The effective model, despite
61 its simplicity, captured key features of ATRA induced differentiation of HL-60 cells. Model
62 analysis predicted the bistability of MAPK activation as a function of ATRA exposure; con-
63 formational experiments supported ATRA-induced bistability. Model simulations were also
64 consistent with measurements of the influence of MAPK inhibitors, and the failure of BLR1
65 knockout cells to differentiate when exposed to ATRA. Lastly, we showed by through im-
66 munoprecipitation studies, that the guanine nucleotide exchange factor Vav1 is potentially
67 a new ATRA-inducible member of the siganlsome complex. Taken together, these findings
68 when combined with other literature evidence, suggested that positive feedback architec-
69 tures are central to differentiation programs generally, and necessary for ATRA-induced
70 differentiation.

71 **Results**

72 We constructed an effective model of ATRA-induced HL-60 differentiation which described
73 signaling and gene expression events following the addition of ATRA (Fig. 1). The model
74 connectivity was developed from literature and the studies presented here (Table 1). We
75 decomposed the ATRA program into three modules; a signal initiation module that sensed
76 and transformed the ATRA signal into activated cRaf-pS621 and the ATRA-RXR/RAR
77 (Trigger) signals (Fig. 1A); a signal integration module that controlled the expression of
78 upstream transcription factors given cRaf-pS621 and activated Trigger signals (Fig. 1B);
79 and a phenotype module which encoded the expression of functional differentiation mark-
80 ers from the ATRA-inducible transcription factors (Fig. 1C). Each component of these
81 modules was described by a mRNA and protein balance equation. Additionally, the sig-
82 nal initiation module also described the abundance of activated species e.g., Trigger and
83 cRaf-pS621 whose values were derived from unactivated Trigger and cRaf protein levels.
84 Lastly, because the population of HL-60 cells was dividing (at least before ATRA-induced
85 cell cycle arrest), we also considered a dilution term in all balance equations. The sig-
86 nal initiation module contained nine differential equations, while the signal integration and
87 phenotype modules were collectively encoded by 54 differential equations. Model param-
88 eters were taken literature (Table 2), or estimated from experimental data using heuristic
89 optimization (see materials and methods).

90 The signal initiation module recapitulated sustained signalsome and MAPK activation
91 following exposure to $1\mu\text{M}$ ATRA (Fig. 2A-B). An ensemble of effective model param-
92 eters was estimated by minimizing the difference between simulations and time-series
93 measurements of BLR1 mRNA and cRaf-pS621 following the addition of $1\mu\text{M}$ ATRA. We
94 focused on the S621 phosphorylation site of cRaf since enhanced phosphorylation at
95 this site is a defining characteristic of sustained MAPK activation in HL-60. The effective
96 model captured both ATRA-induced BLR1 expression (Fig. 2A) and sustained phospho-

97 phosphorylation of cRaf-pS621 (Fig. 2B) in a growing population of HL-60 cells. Together, the
98 reinforcing positive feedback between the signalsome and MAPK led to sustained activation
99 over multiple cellular generations. However, the effective model failed to capture the
100 decline of BLR1 message after 48 hr of ATRA exposure. This suggested that we captured
101 the logic leading to the onset of differentiation, but failed to describe program shutdown.
102 Next, we tested the response of the signal initiation module to different ATRA dosages.

103 The signal initiation model was bistable with respect to ATRA induction (Fig. 2C-D).
104 Phaseplane analysis predicted two stable steady-states when ATRA was present below
105 a critical threshold, and only a single steady-state above the threshold (Fig. 2C). In the
106 lower stable state, neither the signalsome nor cRaf-pS621 were present (thus, the differ-
107 entiation program was deactivated). However, at the high stable state, both the signal-
108 some and cRaf-pS621 were present, allowing for sustained activation and differentiation.
109 Interestingly, when ATRA was above a critical threshold, only the activated state was ac-
110 cessible (Fig. 2D). To test these findings, we first identified the ATRA threshold. We
111 exposed HL-60 cells to different ATRA concentrations for 72 hr (Fig. 2E). Morphological
112 changes associated with differentiation were visible for ATRA \geq 0.25 μ M, suggesting the
113 critical ATRA threshold was near this concentration. Next, we conducted ATRA washout
114 experiments to determine if activated cells remained activated in the absence of ATRA.
115 HL-60 cells locked into an activated state remained activated following ATRA withdraw-
116 (Fig. 3). This sustained activation resulted from reinforcing feedback between the sig-
117 nalsome and the MAPK pathway. Thus, following activation, if we inhibited or removed
118 elements from the signal initiation module we expected the signalsome and MAPK signals
119 to decay. We simulated ATRA induced activation in the presence of kinase inhibitors, and
120 without key circuit elements. Consistent with experimental results using multiple MAPK
121 inhibitors, ATRA activation in the presence of MAPK inhibitors lowered the steady-state
122 value of signalsome (Fig. 3A). In the presence of BLR1, the signalsome and cRaf-pS621

123 signals were maintained following ATRA withdraw (Fig. 3B, gray). On the other hand,
124 BLR1 deletion removed the ability of the circuit to maintain a sustained MAPK response
125 following the withdraw of ATRA (Fig. 3B, blue). Lastly, washout experiments in which
126 cells were exposed to $1\mu\text{M}$ ATRA for 24 hr, and then transferred to fresh media with-
127 out ATRA, confirmed the persistence of the self sustaining activated state for up to 144
128 hr (Fig. 3C). Thus, these experiments confirmed that reinforcing positive feedback likely
129 drives the ATRA-induced differentiation program. Next, we analyzed the ATRA-induced
130 downstream gene expression program following signalsome and cRaf activation.

131 The signal integration and phenotype modules described ATRA-induced gene expres-
132 sion in wild-type HL-60 cells (Fig. 4). The signal initiation module produced two outputs,
133 activated Trigger and cRaf-pS621 which drove the expression of ATRA-induced transcrip-
134 tion factors, which then in turn activated the phenotypic program. In particular, Trigger,
135 which is a surrogate for the RAR α /RXR transcriptional complex, regulated the expres-
136 sion of the transcription factors CCATT/enhancer binding protein α (C/EBP α), PU.1, and
137 EGR1. In turn, these transcription factors, in combination with cRaf-pS621, regulated the
138 expression of downstream phenotypic markers such as CD38, CD11b or P47Phox. We
139 assembled the connectivity of the signal integration and phenotypic programs driven by
140 Trigger and cRaf-pS621 from literature (Table 1). We estimated the parameters which
141 appeared in the control laws regulating these programs from steady-state and dynamic
142 measurements of transcription factor and phenotypic marker expression following the ad-
143 dition of ATRA (22–25). However, the bulk of the remaining model parameters were taken
144 from directly from literature (26) and were not estimated in this study (see materials and
145 methods). The model simulations captured the time dependent expression of CD38 and
146 CD11b following the addition ATRA (Fig. 4A), and the steady-state for signal integration
147 and phenotypic markers (Fig. 4B). Lastly, we used the *predicted* values of the P21 and
148 E2F protein abundance to estimate a blackbox model of ATRA-induced G0 arrest (Fig.

149 5). The phenotype module predicted P21 expression significantly increased and E2F ex-
150 pression decreased, in response to ATRA exposure (Fig. 5A). We then used the ratio of
151 these values in a polynomial model to calculate the fraction of HL-60 cells in G0 arrest
152 following the addition of ATRA (Fig. 5B). The third-order polynomial model captured the
153 trend in measured G0-arrest values as a function of time, and was robust to uncertainty
154 in the measured data (Fig. 5B, gray). Taken together, the output of the signal integra-
155 tion and phenotypic modules was consistent with time-series and steady-state measure-
156 ments, thereby validating the assumed molecular connectivity. Moreover, outputs from
157 the phenotype module described the trend in ATRA-induced G0 cell cycle arrest. Next,
158 we explored which nodes and interactions between nodes in the signal integration module
159 most influenced the system response.

160 The PU.1 and AP1 proteins were critical regulators of the ATRA-induced signal in-
161 tegration and phenotypic programs (Fig. 6). We conducted pairwise knock simulations
162 of genes in the signal integration and phenotype modules to estimate which nodes con-
163 trolled the processing of the Trigger and cRaF-S621 signals. The difference between the
164 system state with and without the gene knockouts (encoded in a state displacement ma-
165 trix) was decomposed using Singular Value Decomposition (SVD). All simulations were
166 conducted using the best fit parameter set. The first four modes described >99% of the
167 gene knockout variance, with the most important components of these modes being the
168 PU.1 and AP1 proteins, and to a much lesser extent GFI1 and CEBPa (Fig. 6A). To better
169 understand which connections involving the PU.1 and AP1 proteins were important, we
170 simulated the pairwise deletion of interactions between these proteins and their respec-
171 tive regulatory targets. SVD decomposition of the state displacement matrix assembled
172 from the pairwise deletion of interactions, suggested the first five modes accounted for
173 >99% of the variance resulting from deletion of the interactions. The most sensitive in-
174 teractions for the PU.1 protein involved the regulation of P47Phox expression, and to a

175 lesser extent AP1 and EGR1 expression (Fig. 6B). On the other other, the most sensitive
176 connections for AP1 involved the regulation of P21 expression, and the mutual activation
177 of PU.1 and AP1 expression. Taken together, these results suggested that the PU.1 and
178 AP1 proteins acted as important regulators for both the signal integration and phenotype
179 modules. However, this analysis did not given insight into which components of the signal
180 initiation module was important, and particularly the nature of the signalsome complex.
181 Toward this question, we experimentally explored the composition and regulation of the
182 signalsome complex.

183 The composition of the siganlsome, and the kinase ultimately responsible for medi-
184 ating ATRA-induced Raf activation is currently unknown. To explore this question, we
185 conducted immunoprecipitation and subsequent Western blotting to identify physical in-
186 teractions between Raf and 19 putative interaction partners. A panel of 19 possible Raf
187 interaction partners (kinases, GTPases, scaffolding proteins etc) was constructed based
188 upon known signaling pathways. We did not consider the most likely binding partner, the
189 small GTPase RAS, as previous studies have ruled it out in MAPK activation in HL-60 cells
190 (20, 27). Total Raf was used as a bait protein for the immunoprecipitation studies. Interro-
191 gation of the Raf interactome suggested Vav1 was involved with ATRA-induced initiation
192 of MAPK activity (Fig. 7). Western blot analysis using total Raf and pS621 Raf specific
193 antibodies confirmed the presence of the bait protein, total and phosphorylated forms, in
194 the immunoprecipitate (Fig. 7A). Of the 19 proteins sampled, Vav1, Src, CK2, Akt, and
195 14-3-3 precipitated with Raf, suggesting a direct physical interaction was possible. How-
196 ever, only the associations between Raf and Vav1 and Raf and Src were ATRA-inducible
197 (Fig. 7). Furthermore, the Vav1 and Src associations were correlated with pS621 Raf
198 abundance in the precipitate. Others proteins e.g., CK2, Akt and 14-3-3, generally bound
199 Raf regardless of phosphorylation status or ATRA treatment. The remaining 14 proteins
200 were expressed in whole cell lysate (Fig. 7B), but were not detectable in the precipitate

201 of Raf IP. Treatment with the Raf kinase inhibitor GW5074 following ATRA exposure re-
202 duced the association of both Vav1 with Raf and Src with Raf (Fig. 7), although the signal
203 intensity for Src was notably weak. However, GW5074 did not influence the association
204 of CK2 or 14-3-3 with Raf, further demonstrating their independence from Raf phospho-
205 rylation. Interestingly, the Raf-Akt interaction qualitatively increased following treatment
206 with GW5074; however, it remained unaffected by treatment with ATRA. Src family ki-
207 nases are known to be important in myeloid differentiation (28) and their role in HL-60
208 differentiation has been investigated elsewhere (11). Given the existing work and variable
209 reproducibility in the context of the Raf immunoprecipitate, we did not investigate the role
210 of Src further in this study. Taken together, the immunoprecipitation and GW5074 results
211 implicated Vav1 association to be correlated with Raf activation following ATRA-treatment.
212 Previous studies demonstrated that a Vav1-Slp76-Cbl-CD38 complex plays an important
213 role in ATRA-induced MAPK activation and differentiation of HL-60 cells (13). Here we
214 did not observe direct interaction of Raf with Cbl or Slp76; however, this complex could
215 be involved upstream. Next, we considered the effect of the Raf kinase inhibitor GW5074
216 on functional markers of ATRA-induced growth arrest and differentiation.

217 Inhibition of Raf kinase activity modulated MAPK activation and differentiation mark-
218 ers following ATRA exposure (Fig. 7D-F). ATRA treatment alone statistically significantly
219 increased the G1/G0 percentage over the untreated control, while GW5074 alone had a
220 negligible effect on the cell cycle distribution (Fig. 7D). Surprisingly, the combination of
221 GW5074 and ATRA statistically significantly increased the G1/G0 population ($82 \pm 1\%$)
222 compared with ATRA alone ($61 \pm 0.5\%$). Increased G1/G0 arrest following the combined
223 treatment with GW5074 and ATRA was unexpected, as the combination of ATRA and the
224 MEK inhibitor (PD98059) has been shown previously to decrease ATRA-induced growth
225 arrest (8). However, growth arrest is not the sole indication of functional differentiation.
226 Expression of the cell surface marker CD11b has also been shown to coincide with HL-60

227 cells myeloid differentiation (29). We measured CD11b expression, for the various treat-
228 ment groups, using immuno-fluorescence flow cytometry 48 hr post-treatment. As with
229 G1/G0 arrest, ATRA alone increased CD11b expression over the untreated control, while
230 GW5074 further enhanced ATRA-induced CD11b expression (Fig. 7E). GW5074 alone
231 had no statistically significant effect on CD11b expression, compared with the untreated
232 control. Lastly, the inducible reactive oxygen species (ROS) response was used as a func-
233 tional marker of differentiated neutrophils (16). We measured the ROS response induced
234 by the phorbol ester 12-O-tetradecanoylphorbol-13-acetate (TPA) using flow cytometry.
235 Untreated cells showed no discernible TPA response, with only $7.0 \pm 3.0\%$ ROS induction
236 (Fig. 7F). Cells treated with ATRA had a significantly increased TPA response, $53 \pm 7\%$
237 ROS induction 48 hr post-treatment. Treatment with both ATRA and GW5074 statistically
238 significantly reduced ROS induction ($22 \pm 0.6\%$) compared to ATRA alone. Interestingly,
239 Western blot analysis did not detect a GW5074 effect on ATRA-induced expression of
240 p47phox, a required upstream component of the ROS response (Fig. 7F, bottom). Thus,
241 the inhibitory effect of GW5074 on inducible ROS might occur downstream of p47phox
242 expression. However, the ROS producing complex is MAPK dependent, therefore it is
243 also possible that GW5074 inhibited ROS production by interfering with MAPK activation
244 (in which case the p47Phox marker might not accurately reflect phenotypic conversion
245 and differentiation).

246 **Discussion**

247 In this study, we presented an effective model of ATRA-inducible differentiation of HL-60
248 cells which encoded positive feedback between the ATRA-inducible signalsome complex
249 and the MAPK pathway. Despite its simplicity, the model captured key features of the
250 ATRA induced differentiation such as sustained MAPK activation, and bistability with re-
251 spect to ATRA exposure. We also reported a new ATRA-inducible component of the
252 signalsome, Vav1. Vav1 is a guanine nucleotide exchange factor for Rho family GTPases
253 that activate pathways leading to actin cytoskeletal rearrangements and transcriptional al-
254 terations (30). The Vav1/Raf association correlated with Raf activity, was ATRA-inducible
255 and decreased after treatment with GW5074. The presence of Vav1 in Raf/Grb2 com-
256 plexes has been shown to correlate with increased Raf activity in mast cells (31). Fur-
257 thermore, studies on Vav1 knockout mice demonstrated that the loss of Vav1 resulted
258 in deficiencies of ERK signaling for both T-cells as well as neutrophils (32, 33). While its
259 function in the signalsome is unclear, Vav1 has been shown to associate with a Cbl-Slp76-
260 CD38 complex in an ATRA-dependent manner; furthermore, transfection of HL-60 cells
261 with Cbl mutants that fail to bind CD38, yet still bind Slp76 and Vav1, prevented ATRA-
262 induced MAPK activation (13). Thus, interaction of Cbl-Slp76-Vav1 and CD38 appears to
263 be required for transmission of the ATRA signal by the signalsome.

264 We conducted immunoprecipitation studies and identified a limited number of ATRA-
265 dependent and -independent Raf interaction partners. While we were unable to detect
266 the association of Raf with common kinases and GTPases such as PKC, PKA, p38, Rac
267 and Rho, we did establish potential interactions between Raf and key partners such as
268 Vav1, Src, Akt, CK2 and 14-3-3. All of these partners are known to be associated with Raf
269 activation or function. Src is known to bind Raf through an SH2 domain, and this associ-
270 ation has been shown to be dependent of the serine phosphorylation of Raf (34). Thus,
271 an ATRA inducible Src/Raf association may be a result of ATRA-induced Raf phospho-

272 rylation at S259 or S621. We also identified an interaction between Raf and the Ser/Thr
273 kinases Akt and CK2. Akt can phosphorylate Raf at S259, as demonstrated by studies
274 in a human breast cancer line (35). CK2 can also phosphorylate Raf, although the lit-
275 erature has traditionally focused on S338 and not S621 or S259(36). However, neither
276 of these kinase interactions were ATRA-inducible, suggesting their association with Raf
277 alone was not associated with ATRA-induced Raf phosphorylation. The adapter protein
278 14-3-3 was also constitutively associated with Raf. The interaction between Raf and 14-
279 3-3 has been associated with both S621 and S259 phosphorylation and activity (37).
280 Additionally, the association of Raf with 14-3-3 not only stabilized S621 phosphorylation,
281 but also reversed the S621 phosphorylation from inhibitory to activating (38). Finally, we
282 found that Vav1/Raf association correlated with Raf activity, was ATRA-inducible and de-
283 creased after treatment with GW5074. The presence of Vav1 in Raf/Grb2 complexes has
284 been shown to correlate with increased Raf activity in mast cells (31). Furthermore, stud-
285 ies on Vav1 knockout mice demonstrated that the loss of Vav1 resulted in deficiencies of
286 ERK signaling for both T-cells as well as neutrophils (32, 33). Interestingly, while an in-
287 tegrin ligand-induced ROS response was blocked in Vav1 knockout neutrophils, TPA was
288 able to bypass the Vav1 requirement and stimulate both ERK phosphorylation and ROS
289 induction (33). In this study, the TPA-induced ROS response was dependent upon Raf
290 kinase activity, and was mitigated by the addition of GW5074. It is possible that Vav1 is
291 downstream of various integrin receptors but upstream of Raf in terms of inducible ROS
292 responses. Vav1 has also been shown to associate with a Cbl-Slp76-CD38 complex in an
293 ATRA-dependent manner; furthermore, transfection of HL-60 cells with Cbl mutants that
294 fail to bind CD38, yet still bind Slp76 and Vav1, prevents ATRA-induced MAPK activation
295 (13). The literature suggest a variety of possible receptor-signaling pathways, which in-
296 volve Vav1, for MAPK activation; moreover, given the ATRA-inducible association Vav1
297 may play a direct role in Raf activation.

298 We hypothesized that Vav1 is a member of an ATRA-inducible complex which propels
299 sustained MAPK activation, arrest and differentiation. Initially, ATRA-induced Vav1 ex-
300 pression drives increased association between Vav1 and Raf. This increased interaction
301 facilitates phosphorylation and activation of Raf by pre-bound Akt and/or CK2 at S621
302 or perhaps S259. Constitutively bound 14-3-3 may also stabilize the S621 phosphory-
303 lation, modulate the activity and/or up-regulate autophosphorylation. Activated Raf can
304 then drive ERK activation, which in turn closes the positive feedback loop by activating
305 Raf transcription factors, e.g. Sp1 and/or STAT1 (39–42). We tested this working hy-
306 pothesis using mathematical modeling. The model recapitulated both ATRA time-course
307 data as well as the GW5074 inhibitor effects. This suggested the proposed Raf-Vav1
308 architecture was at least consistent with the experimental studies. Further, analysis of
309 the Raf-Vav1 model identified bistability in ppERK levels. Thus, two possible MAPK ac-
310 tivation branches were possible for experimentally testable ATRA values. The analysis
311 also suggested the ATRA-induced Raf-Vav1 architecture could be locked into a sustained
312 signaling mode (high ppERK) even in the absence of a ATRA signal. This locked-in prop-
313 erty could give rise to an ATRA-induction memory. We validated the treatment memory
314 property predicted by the Raf-Vav1 circuit experimentally using ATRA-washout experi-
315 ments. ERK phosphorylation levels remained high for more then 96 hr after ATRA was
316 removed. Previous studies demonstrated that HL-60 cells possessed an inheritable mem-
317 ory of ATRA stimulus (43). Although the active state was self-sustaining, the inactive state
318 demonstrated considerable robustness to perturbation. For example, we found that 50x
319 overexpression of Raf was required to reliably lock MAPK into the activated state, while
320 small perturbations had almost no effect on ppERK levels over the entire ensemble. CD38
321 expression correlated with the ppERK, suggesting its involvement in the signaling com-
322 plex. Our computational and experimental results showed that positive feedback, through
323 ERK-dependent Raf expression, could sustain MAPK signaling through many division cy-

324 cles. Such molecular mechanisms could underly aspects of cellular memory associated
325 to consecutive ATRA treatments.

326 Several engineered, or naturally occurring systems involved in cell fate decisions incor-
327 porate positive feedback and bistability (44). One of the most well studied cell fate circuits
328 is the Mos mitogen-activated protein kinase cascade in *Xenopus* oocytes. This cascade
329 is activated when oocytes are induced by the steroid hormone progesterone (45). The
330 MEK-dependent activation of p42 MAPK stimulates the accumulation of the Mos onco-
331 protein, which in turn activates MEK, thereby closing the feedback loop. This is similar to
332 the differentiation circuit presented here; ATRA drives signalsome which activates MAPK,
333 cell-cycle arrest, differentiation and signalsome. Thus, while HL-60 and *Xenopus* oocytes
334 are vastly different biological models, they share similar cell fate decision architectures.
335 Other unrelated cell fate decisions such as programmed cell death have also been sug-
336 gested to be bistable (46). Still more biochemical networks important to human health,
337 for example the human coagulation or complement cascades, also feature strong positive
338 feedback elements (47). Thus, while positive feedback is sometimes not desirable in man-
339 made systems, it may be at the core of a diverse variety of cell fate programs and other
340 networks important to human health.

341 Model performance was impressive given its limited size. However, there were several
342 issues to explore further. First, there was likely missing connectivity in the effective differ-
343 entiation circuit. Decreasing BLR1 expression with simultaneously sustained cRaf-pS261
344 activation was not captured by the current network architecture. This suggested that
345 signalsome, once activated, had a long lifetime as decreased BLR1 expression did not
346 impact cRaf-pS261 abundance. We could model this by separating signalsome formation
347 into an inactive precursor pool that is transformed to a long-lived activated signalsome by
348 MAPK activation. We should also explore adding additional downstream biological mod-
349 ules to this skeleton model, for example the upregulation of reactive oxygen markers such

350 as p47Phox or cell cycle arrest components to capture the switch from an actively prolif-
351 erating population to a population in G0-arrest. Next, the choice of max/min integration
352 rules or the particular form of the transfer functions could also be explored. Integration
353 rules other than max/min could be used, such as the mean or the product, assuming the
354 range of the transfer functions is always $f \in [0, 1]$. Alternative integration rules might
355 have different properties which could influence model identification or performance. For
356 example, a mean integration rule would be differentiable, allowing derivative-based opti-
357 mization approaches to be used. The form of the transfer function could also be explored.
358 We choose hill-like functions because of their prominence in the systems and synthetic
359 biology community. However, many other transfer functions are possible.

360 **Materials and Methods**

361 *Effective gene expression model equations.* We decomposed the ATRA-induced differ-
 362 entiation program into three modules; a signal initiation module that sensed and trans-
 363 formed the ATRA signal into activated cRaf-pS621 and the ATRA-RXR/RAR (activated
 364 Trigger) signals; a signal integration module that controlled the expression of upstream
 365 transcription factors given cRaf-pS621 and activated Trigger signals; and a phenotype
 366 module which encoded the expression of functional differentiation markers from the ATRA-
 367 inducible transcription factors. The output of the signal initiation module was the input to
 368 the gene expression model. For each gene $j = 1, 2, \dots, \mathcal{G}$, we modeled both the mRNA
 369 (m_j), protein (p_j) and signaling species abundance:

$$\frac{dm_j}{dt} = r_{T,j} - (\mu + \theta_{m,j}) m_j + \lambda_j \quad (1)$$

$$\frac{dp_j}{dt} = r_{X,j} - (\mu + \theta_{p,j}) p_j \quad (2)$$

$$g(p_1, \dots, p_{\mathcal{G}}, \kappa) = 0 \quad (3)$$

370 The terms $r_{T,j}$ and $r_{X,j}$ denote the specific rates of transcription, and translation while
 371 the terms $\theta_{m,j}$ and $\theta_{p,j}$ denote first-order degradation constants for mRNA and protein,
 372 respectively. The specific transcription rate $r_{T,j}$ was modeled as the product of a kinetic
 373 term $\bar{r}_{T,j}$ and a control term u_j which described how the abundance of transcription fac-
 374 tors, or other regulators influenced the expression of gene j . The kinetic transcription
 375 term $\bar{r}_{T,j}$ was modeled as:

$$\bar{r}_{T,j} = V_T^{max} \left(\frac{L_{T,o}}{L_{T,j}} \right) \left(\frac{G_j}{K_T + G_j} \right) \quad (4)$$

376 where the maximum gene expression rate V_T^{max} was defined as the product of a char-
 377 acteristic transcription rate constant (k_T) and the abundance of RNA polymerase (R_1),

378 $V_T^{max} = k_T(R_1)$. The $(L_{T,o}/L_{T,j})$ term denotes the ratio of transcription read lengths; $L_{T,o}$
 379 represents a characteristic gene length, while $L_{T,j}$ denotes the length of gene j . Thus,
 380 the ratio $(L_{T,o}/L_{T,j})$ is a gene specific correction to the characteristic transcription rate
 381 V_T^{max} . The degradation rate constants were defined as $\theta_{m,j}$ and $\theta_{p,j}$ denote characteristic
 382 degradation constants for mRNA and protein, respectively. Lastly, the λ_j term denotes the
 383 constitutive rate of expression of gene j .

384 The gene expression control term $0 \leq u_j \leq 1$ depended upon the combination of fac-
 385 tors which influenced the expression of gene j . If the expression of gene j was influenced
 386 by $1, \dots, m$ factors, we modeled this relationship as $u_j = \mathcal{I}_j(f_{1j}(\cdot), \dots, f_{mj}(\cdot))$ where
 387 $0 \leq f_{ij}(\cdot) \leq 1$ denotes a regulatory transfer function quantifying the influence of factor i
 388 on the expression of gene j , and $\mathcal{I}_j(\cdot)$ denotes an integration rule which combines the
 389 individual regulatory inputs for gene j into a single control term. In this study, the integra-
 390 tion rule governing gene expression was the weighted fraction of promoter configurations
 391 that resulted in gene expression (48):

$$u_j = \frac{W_{R_{1,j}} + \sum_n W_{nj} f_{nj}}{1 + W_{R_{1,j}} + \sum_d W_{dj} f_{dj}} \quad (5)$$

392 The numerator, the weighted sum (with weights W_{nj}) of promoter configurations leading to
 393 gene expression, was normalized by all possible promoter configurations. The likelihood
 394 of each configuration was quantified by the transfer function f_{nj} (which we modeled using
 395 hill like functions), while the lead term in the numerator $W_{R_{1,j}}$ denotes the weight of con-
 396 stitutive expression for gene j . Given this formulation, the rate of constitutive expression
 397 was then given by:

$$\lambda_j = \bar{r}_{T,j} \left(\frac{W_{R_{1,j}}}{1 + W_{R_{1,j}}} \right) \quad (6)$$

398 If a gene expression process had no modifying factors, $u_j = 1$. Lastly, the specific trans-

399 lation rate was modeled as:

$$r_{X,j} = V_X^{\max} \left(\frac{L_{X,o}}{L_{X,j}} \right) \left(\frac{m_j}{K_X + m_j} \right) \quad (7)$$

400 where V_X^{\max} denotes a characteristic maximum translation rate estimated from literature,
401 and K_X denotes a translation saturation constant. The characteristic maximum translation
402 rate was defined as the product of a characteristic translation rate constant (k_X) and
403 the Ribosome abundance (R_2), $V_X^{\max} = k_X (R_2)$. As was the case for transcription, we
404 corrected the characteristic translation rate by the ratio of the length of a characteristic
405 transcription normalized by the length of transcript j .

406 *Signaling model equations.* The signal initiation, and integration modules required the
407 abundance of cRaf-pS621 and ATRA-RXR/RAR (activated Trigger) as inputs. However,
408 our base model described only the abundance of inactive proteins e.g., cRaf or RXR/RAR
409 but not the activated forms. To address this issue, we estimated pseudo steady state
410 approximations for the abundance of cRaf-pS621 and activated Trigger (shown generally
411 as Eq (3)). The abundance of activated trigger ($x_{a,1}$) was estimated directly from the
412 RXR/RAR abundance ($x_{u,1}$):

$$x_{a,1} \sim x_{u,1} \left(\frac{\alpha \cdot \text{ATRA}}{1 + \alpha \cdot \text{ATRA}} \right) \quad (8)$$

413 where α denotes a gain parameter; $\alpha = 0.0$ if ATRA is less than a threshold, and $\alpha = 0.1$
414 if ATRA is greater than the differentiation threshold. The abundance of cRaf-pS621 was
415 estimated by making the pseudo steady state approximation on the cRaf-pS621 balance.
416 The abundance of an activated signaling species i was given by:

$$\frac{dx_i}{dt} = r_{+,i}(\mathbf{x}, \mathbf{k}) - (\mu + k_{d,i}) x_i \quad i = 1, \dots, \mathcal{M} \quad (9)$$

417 The quantity x_i denotes concentration of signaling species i , while \mathcal{R} and \mathcal{M} denote
 418 the number of signaling reactions and signaling species in the model, respectively. The
 419 term $r_{+,i}(\mathbf{x}, \mathbf{k})$ denotes the rate of generation of activated species i , while μ denotes
 420 the specific growth rate, and $k_{d,i}$ denotes the rate constant controlling the non-specific
 421 degradation of x_i . We neglected deactivation reactions e.g., phosphatase activities. We
 422 assumed that signaling processes were fast compared to gene expression; this allowed
 423 us to approximate the signaling balance as:

$$x_i^* \simeq \frac{r_{+,i}(\mathbf{x}, \mathbf{k})}{(\mu + k_{d,i})} \quad i = 1, \dots, \mathcal{M} \quad (10)$$

424 The generation rate was written as the product of a kinetic term ($\bar{r}_{+,i}$) and a control term
 425 (v_i). The control terms $0 \leq v_j \leq 1$ depended upon the combination of factors which in-
 426 fluenced rate process j . If rate j was influenced by $1, \dots, m$ factors, we modeled this
 427 relationship as $v_j = \mathcal{I}_j(f_{1j}(\cdot), \dots, f_{mj}(\cdot))$ where $0 \leq f_{ij}(\cdot) \leq 1$ denotes a regulatory
 428 transfer function quantifying the influence of factor i on rate j . The function $\mathcal{I}_j(\cdot)$ is an
 429 integration rule which maps the output of regulatory transfer functions into a control vari-
 430 able. In this study, we used $\mathcal{I}_j \in \{\min, \max\}$ and hill transfer functions (49). If a process
 431 had no modifying factors, $v_j = 1$. The kinetic rate of cRaf-pS621 generation $\bar{r}_{+,cRaf}$ was
 432 modeled as:

$$\bar{r}_{+,cRaf} = k_{+,cRaf} x_s \left(\frac{x_{cRaf}}{K_{+,cRaf} + x_{cRaf}} \right) \quad (11)$$

433 where x_s denotes the signalsome abundance, and $K_{+,cRaf}$ denotes a saturation constant
 434 governing cRaf-pS621 formation. The formation of cRaf-pS621 was regulated by only a
 435 single factor, the abundance of MAPK inhibitor, thus $v_{+,cRaf}$ took the form:

$$v_{+,cRaf} = \left(1 - \frac{I}{K_D + I} \right) \quad (12)$$

436 where I denotes the abundance of the MAPK inhibitor, and K_D denotes the inhibitor
437 affinity.

438 *Estimation of gene expression model parameters.* We estimated parameters appearing
439 in the mRNA and protein balances, the abundance of polymerases and ribosomes, tran-
440 scription and translation rates, the half-life of a typical mRNA and protein, and typical
441 values for the copies per cell of RNA polymerase and ribosomes from literature (Table 2).
442 The saturation constants K_X and K_T were adjusted so that gene expression and trans-
443 lation resulted in gene products on a biologically realistic concentration scale. Lastly, we
444 calculated the concentration for gene G_j by assuming, on average, that a cell had two
445 copies of each gene at any given time. Thus, the bulk of our gene expression model pa-
446 rameters were based directly upon literature values, and were not adjusted during model
447 identification. However, the remaining parameters, e.g., the W_{ij} appearing in the gene
448 expression control laws, or parameters appearing in the transfer functions f_{dij} , were esti-
449 mated from the protein expression and signaling data sets discussed here.

450 Signaling and gene expression model parameters were estimated by minimizing the
451 squared difference between simulations and experimental protein data set j . We mea-
452 sured the squared difference in the scale, fold change and shape for protein j :

$$E_j(\mathbf{k}) = \left(\mathcal{M}_j(t_-) - \hat{y}_j(t_-, \mathbf{k}) \right)^2 + \sum_{i=1}^{\mathcal{T}_j} \left(\hat{\mathcal{M}}_{ij} - \hat{y}_{ij}(\mathbf{k}) \right)^2 + \sum_{i=1}^{\mathcal{T}_j} \left(\mathcal{M}'_{ij} - y'_{ij}(\mathbf{k}) \right)^2 \quad (13)$$

453 The first term in Eqn. (13) quantified the initial *scale* error, directly before the addition
454 of ATRA. In this case, $\mathcal{M}_j(t_-)$ (the approximate concentration of protein j before the
455 addition of ATRA) was estimated from literature. This term was required because the
456 protein measurements were reported as the fold-change; thus, the data was normalized
457 by a control value measured before the addition of ATRA. However, the model operated on
458 a physical scale. The first term allowed the model to capture physically realistic changes

following ATRA addition. The second term quantified the difference in the *fold-change* of protein j as a function of time. The terms $\hat{\mathcal{M}}_{ij}$ and \hat{y}_{ij} denote the scaled experimental observations and simulation outputs (fold-change; protein normalized by control value directly before ATRA addition) at time i from protein j , where T_j denoted the number of time points for data set j . Lastly, the third term of the objective function measured the difference in the *shape* of the measured and simulated protein levels. The scaled value $0 \leq \mathcal{M}'_{ij} \leq 1$ was given by:

$$\hat{\mathcal{M}}_{ij} = \left(\mathcal{M}_{ij} - \min_i \mathcal{M}_{ij} \right) / \left(\max_i \mathcal{M}_{ij} - \min_i \mathcal{M}_{ij} \right) \quad (14)$$

where $\mathcal{M}'_{ij} = 0$ and $\mathcal{M}'_{ij} = 1$ describe the lowest (highest) intensity bands. A similar scaling was used for the simulation output. We minimized the total model residual $\sum_j E_j$ using a heuristic direct-search optimization procedure, subject to box constraints on the parameter values, starting from a random initial parameter guess. Each downhill step was archived and used for ensemble calculations. The optimization procedure (a covariance matrix adaptation evolution strategy) has been reported previously (50).

Estimation of an effective cell cycle arrest model. We formulated an effective N-order polynomial model of the fraction of cells undergoing ATRA-induced cell cycle arrest at time t , $\hat{\mathcal{A}}(t)$, as:

$$\hat{\mathcal{A}}(t) \simeq a_0 + \sum_{i=1}^{N-1} a_i \phi_i(\mathbf{p}(t), t) \quad (15)$$

where a_i were unknown parameters, and $\phi_i(\mathbf{p}(t), t)$ denotes a basis function. The basis functions were dependent upon the system state; in this study, we assumed $N = 4$ and basis functions of the form:

$$\phi_i(\mathbf{p}(t), t) = \left(\frac{t}{T} + \frac{p21}{E2F} \Big|_t \right)^{(i-1)} \quad (16)$$

478 The parameters a_0, \dots, a_3 were estimated directly from cell-cycle measurements (biologi-
479 cal replicates) using least-squares.

480 *Availability of model code.* The signaling and gene expression model equations, and the
481 parameter estimation procedure, were implemented in the Julia programming language.
482 The model equations were solved using the ODE23s routine of the ODE package (51). The
483 model code and parameter ensemble is freely available under an MIT software license
484 and can be downloaded from <http://www.varnerlab.org>.

485 *Cell culture and treatment* Human myeloblastic leukemia cells (HL-60 cells) were grown
486 in a humidified atmosphere of 5% CO₂ at 37°C and maintained in RPMI 1640 from Gibco
487 (Carlsbad, CA) supplemented with 5% heat inactivated fetal bovine serum from Hyclone
488 (Logan, UT) and 1× antibiotic/antimicotic (Gibco, Carlsbad, CA). Cells were cultured in
489 constant exponential growth (52). Experimental cultures were initiated at 0.1×10^6 cells/mL
490 24 hr prior to ATRA treatment; if indicated, cells were also treated with GW5074 (2 μ M) 18
491 hr before ATRA treatment. For the cell culture washout experiments, cells were treated
492 with ATRA for 24 hr, washed 3x with prewarmed serum supplemented culture medium
493 to remove ATRA, and reseeded in ATRA-free media as described. Western blot analysis
494 was performed at incremental time points after removal of ATRA.

495 *Chemicals* All-Trans Retinoic Acid (ATRA) from Sigma-Aldrich (St. Louis, MO) was dis-
496 solved in 100% ethanol with a stock concentration of 5mM, and used at a final concen-
497 tration of 1 μ M (unless otherwise noted). The cRaf inhibitor GW5074 from Sigma-Aldrich
498 (St. Louis, MO) was dissolved in DMSO with a stock concentration of 10mM, and used
499 at a final concentration of 2 μ M. HL-60 cells were treated with 2 μ M GW5074 with or with-
500 out ATRA (1 μ M) at 0 hr. This GW5074 dosage had a negligible effect on the cell cycle
501 distribution, compared to ATRA treatment alone.

502 *Immunoprecipitation and western blotting* Approximately 1.2×10^7 cells were lysed using
503 $400\mu\text{L}$ of M-Per lysis buffer from Thermo Scientific (Waltham, MA). Lysates were cleared
504 by centrifugation at $16,950 \times g$ in a micro-centrifuge for 20 min at 4°C . Lysates were
505 pre-cleared using $100\mu\text{L}$ protein A/G Plus agarose beads from Santa Cruz Biotechnology
506 (Santa Cruz, CA) by inverting overnight at 4°C . Beads were cleared by centrifugation and
507 total protein concentration was determined by a BCA assay (Thermo Scientific, Waltham,
508 MA). Immunoprecipitations were setup by bringing lysate to a concentration of 1g/L in a
509 total volume of $300\mu\text{L}$ (M-Per buffer was used for dilution). The anti-Raf antibody was
510 added at $3\mu\text{L}$. A negative control with no bait protein was also used to exclude the di-
511 rect interaction of proteins with the A/G beads. After 1 hr of inversion at 4°C , $20\mu\text{L}$ of
512 agarose beads was added and samples were left to invert overnight at 4°C . Samples
513 were then washed three times with M-Per buffer by centrifugation. Finally proteins were
514 eluted from agarose beads using a laemmli loading buffer. Eluted proteins were resolved
515 by SDS-PAGE and Western blotting. Total lysate samples were normalized by total protein
516 concentration ($20\mu\text{g}$ per sample) and resolved by SDS-PAGE and Western blotting. Sec-
517 ondary HRP bound antibody was used for visualization. All antibodies were purchased
518 from Cell Signaling (Boston, MA) with the exception of α -p621 Raf which was purchased
519 from Biosource/Invitrogen (Carlsbad, CA), and α -CK2 from BD Biosciences (San Jose,
520 CA).

521 *Morphology assessment* Untreated and ATRA-treated HL-60 cells were collected after
522 72 hr and cytocentrifuged for 3 min at 700 rpm onto glass slides. Slides were air-dried
523 and stained with Wright's stain. Slide images were captured at 40X (Leica DM LB 100T
524 microscope, Leica Microsystems).

525 **Competing interests**

526 The authors declare that they have no competing interests.

527 **Author's contributions**

528 J.V and A.Y directed the study. R.T, H.J, R.B and J.C conducted the cell culture measure-
529 ments. J.V, R.B, W.D, K.R and A.S developed the reduced order HL-60 models and the
530 parameter ensemble. W.D and J.V analyzed the model ensemble, and generated figures
531 for the manuscript. The manuscript was prepared and edited for publication by W.D, A.Y
532 and J.V.

533 **Acknowledgements**

534 We gratefully acknowledge the suggestions from the anonymous reviewers to improve
535 this manuscript.

536 **Funding**

537 We acknowledge the financial support to J.V. by the National Science Foundation CA-
538 REER (CBET-0846876) for the support of R.T. and H.J. In addition, we acknowledge
539 support to A.Y. from the National Institutes of Health (CA 30555, CA152870) and a grant
540 from New York State Stem Cell Science. Lastly, we acknowledge the financial support to
541 J.V. and A.Y. from the National Cancer Institute (#U54 CA143876). The content is solely
542 the responsibility of the authors and does not necessarily represent the official views of
543 the National Cancer Institute or the National Institutes of Health.

544 **References**

- 545 1. Bushue N, Wan YJY (2010) Retinoid pathway and cancer therapeutics. *Adv Drug
546 Deliv Rev* 62: 1285-98.
- 547 2. Tang XH, Gudas LJ (2011) Retinoids, retinoic acid receptors, and cancer. *Annu Rev
548 Pathol* 6: 345-64.
- 549 3. Cheung FSG, Lovicu FJ, Reichardt JKV (2012) Current progress in using vitamin d
550 and its analogs for cancer prevention and treatment. *Expert Rev Anticancer Ther*
551 12: 811-37.
- 552 4. Nilsson B (1984) Probable in vivo induction of differentiation by retinoic acid of
553 promyelocytes in acute promyelocytic leukaemia. *Br J Haematol* 57: 365-71.
- 554 5. Warrell RP Jr (1993) Retinoid resistance in acute promyelocytic leukemia: new
555 mechanisms, strategies, and implications. *Blood* 82: 1949-53.
- 556 6. Freemantle SJ, Spinella MJ, Dmitrovsky E (2003) Retinoids in cancer therapy and
557 chemoprevention: promise meets resistance. *Oncogene* 22: 7305-15.
- 558 7. Breitman TR, Selonick SE, Collins SJ (1980) Induction of differentiation of the hu-
559 man promyelocytic leukemia cell line (HL-60) by retinoic acid. *Proc Natl Acad Sci U
560 S A* 77: 2936–2940.
- 561 8. Yen A, Roberson MS, Varvayanis S, Lee AT (1998) Retinoic acid induced
562 mitogen-activated protein (MAP)/extracellular signal-regulated kinase (ERK) kinase-
563 dependent MAP kinase activation needed to elicit HL-60 cell differentiation and
564 growth arrest. *Cancer Res* 58: 3163–3172.
- 565 9. Hong HY, Varvayanis S, Yen A (2001) Retinoic acid causes MEK-dependent RAF
566 phosphorylation through RARalpha plus RXR activation in HL-60 cells. *Differentia-
567 tion* 68: 55–66.
- 568 10. Mangelsdorf DJ, Ong ES, Dyck JA, Evans RM (1990) Nuclear receptor that identifies
569 a novel retinoic acid response pathway. *Nature* 345: 224–229.

- 570 11. Congleton J, MacDonald R, Yen A (2012) Src inhibitors, PP2 and dasatinib, increase
571 retinoic acid-induced association of Lyn and c-Raf (S259) and enhance MAPK-
572 dependent differentiation of myeloid leukemia cells. Leukemia 26: 1180-8.
- 573 12. Shen M, Bunaci R, Congleton J, Jensen H, Sayam L, et al. (2011) Interferon regu-
574 latory factor-1 binds c-Cbl, enhances mitogen activated protein kinase signaling and
575 promotes retinoic acid-induced differentiation of HL-60 human myelo-monoblastic
576 leukemia cells. Leuk Lymphoma 52: 2372-9.
- 577 13. Shen M, Yen A (2009) c-Cbl tyrosine kinase-binding domain mutant G306E abol-
578 ishes the interaction of c-Cbl with CD38 and fails to promote retinoic acid-induced
579 cell differentiation and G0 arrest. J Biol Chem 284: 25664–25677.
- 580 14. Yen A, Varvayanis S, Smith J, Lamkin T (2006) Retinoic acid induces expression of
581 SLP-76: expression with c-FMS enhances ERK activation and retinoic acid-induced
582 differentiation/G0 arrest of HL-60 cells. Eur J Cell Biol 85: 117–132.
- 583 15. Marchisio M, Bertagnolo V, Colamussi ML, Capitani S, Neri LM (1998) Phos-
584 phatidylinositol 3-kinase in HL-60 nuclei is bound to the nuclear matrix and increases
585 during granulocytic differentiation. Biochem Biophys Res Commun 253: 346-51.
- 586 16. Congleton J, Jiang H, Malavasi F, Lin H, Yen A (2011) ATRA-induced HL-60 myeloid
587 leukemia cell differentiation depends on the CD38 cytosolic tail needed for mem-
588 brane localization, but CD38 enzymatic activity is unnecessary. Exp Cell Res 317:
589 910–919.
- 590 17. Wang J, Yen A (2004) A novel retinoic acid-responsive element regulates retinoic
591 acid induced BLR1 expression. Mol Cell Biol 24: 2423 - 2443.
- 592 18. Yen A (1990) HL-60 cells as a model of growth and differentiation: the significance
593 of variant cells. Hematology Review 4: 5-46.
- 594 19. Yang T, Xiong Q, Enslen H, Davis R, Chow CW (2002) Phosphorylation of NFATc4
595 by p38 mitogen-activated protein kinases. Mol Cell Biol 22: 3892–3904.

- 596 20. Wang J, Yen A (2008) A MAPK-positive Feedback Mechanism for BLR1 Signaling
597 Propels Retinoic Acid-triggered Differentiation and Cell Cycle Arrest. *J Biol Chem*
598 283: 4375–4386.
- 599 21. Tasseff R, Nayak S, Song S, Yen A, Varner J (2011) Modeling and analysis of retinoic
600 acid induced differentiation of uncommitted precursor cells. *Integr Biol* 3: 578 - 591.
- 601 22. Jensen HA, Styskal LE, Tasseff R, Bunaciu RP, Congleton J, et al. (2013) The
602 src-family kinase inhibitor pp2 rescues inducible differentiation events in emergent
603 retinoic acid-resistant myeloblastic leukemia cells. *PLoS One* 8: e58621.
- 604 23. Jensen HA, Bunaciu RP, Ibabao CN, Myers R, Varner JD, et al. (2014) Retinoic acid
605 therapy resistance progresses from unilineage to bilineage in hl-60 leukemic blasts.
606 *PLoS One* 9: e98929.
- 607 24. Jensen HA, Bunaciu RP, Varner JD, Yen A (2015) Gw5074 and pp2 kinase inhibitors
608 implicate nontraditional c-raf and lyn function as drivers of retinoic acid-induced mat-
609 uration. *Cell Signal* 27: 1666-75.
- 610 25. Jensen HA, Yourish HB, Bunaciu RP, Varner JD, Yen A (2015) Induced myelomono-
611 cytic differentiation in leukemia cells is accompanied by noncanonical transcription
612 factor expression. *FEBS Open Bio* 5: 789-800.
- 613 26. Milo R, Jorgensen P, Moran U, Weber G, Springer M (2010) Bionumbers—the
614 database of key numbers in molecular and cell biology. *Nucleic Acids Res* 38: D750-
615 3.
- 616 27. Katagiri K, Hattori S, Nakamura S, Yamamoto T, Yoshida T, et al. (1994) Activation
617 of ras and formation of gap complex during tpa-induced monocytic differentiation of
618 hl-60 cells. *Blood* 84: 1780–1789.
- 619 28. Miranda MB, Johnson DE (2007) Signal transduction pathways that contribute to
620 myeloid differentiation. *Leukemia* 21: 1363–1377.
- 621 29. Hickstein DD, Back AL, Collins SJ (1989) Regulation of expression of the cd11b and

- 622 cd18 subunits of the neutrophil adherence receptor during human myeloid differen-
623 tiation. *J Biol Chem* 264: 21812–21817.
- 624 30. Hornstein I, Alcover A, Katzav S (2004) Vav proteins, masters of the world of cy-
625 toskeleton organization. *Cell Signal* 16: 1-11.
- 626 31. Song JS, Gomez J, Stancato LF, Rivera J (1996) Association of a p95 vav-containing
627 signaling complex with the fcepsilonlonri gamma chain in the rbl-2h3 mast cell line.
628 evidence for a constitutive in vivo association of vav with grb2, raf-1, and erk2 in an
629 active complex. *J Biol Chem* 271: 26962–26970.
- 630 32. Costello PS, Walters AE, Mee PJ, Turner M, Reynolds LF, et al. (1999) The rho-
631 family gtp exchange factor vav is a critical transducer of t cell receptor signals to the
632 calcium, erk, and nf-kappab pathways. *Proc Natl Acad Sci U S A* 96: 3035–3040.
- 633 33. Graham D, Robertson C, Bautista J, Mascarenhas F, Diacovo M, et al. (2007)
634 Neutrophil-mediated oxidative burst and host defense are controlled by a Vav-
635 PLCgamma2 signaling axis in mice. *J Clin Invest* 117: 3445–3452.
- 636 34. Cleghon V, Morrison DK (1994) Raf-1 interacts with fyn and src in a non-
637 phosphotyrosine-dependent manner. *J Biol Chem* 269: 17749–17755.
- 638 35. Zimmermann S, Moelling K (1999) Phosphorylation and regulation of raf by akt (pro-
639 tein kinase b). *Science* 286: 1741–1744.
- 640 36. Ritt DA, Zhou M, Conrads TP, Veenstra TD, Copeland TD, et al. (2007) Ck2 is a
641 component of the ksr1 scaffold complex that contributes to raf kinase activation.
642 *Curr Biol* 17: 179–184.
- 643 37. Hekman M, Wiese S, Metz R, Albert S, Troppmair J, et al. (2004) Dynamic changes
644 in c-raf phosphorylation and 14-3-3 protein binding in response to growth factor stim-
645 ulation: differential roles of 14-3-3 protein binding sites. *J Biol Chem* 279: 14074–
646 14086.
- 647 38. Dhillon AS, Yip YY, Grindlay GJ, Pakay JL, Dangers M, et al. (2009) The c-terminus

- 648 of raf-1 acts as a 14-3-3-dependent activation switch. *Cell Signal* 21: 1645–1651.
- 649 39. Kim HS, Lim IK (2009) Phosphorylated extracellular signal-regulated protein kinases
- 650 1 and 2 phosphorylate sp1 on serine 59 and regulate cellular senescence via tran-
- 651 scription of p21sdi1/cip1/waf1. *J Biol Chem* 284: 15475–15486.
- 652 40. Milanini-Mongiat J, Pouyss?gur J, Pag? G (2002) Identification of two sp1 phos-
- 653 phorylation sites for p42/p44 mitogen-activated protein kinases: their implication in
- 654 vascular endothelial growth factor gene transcription. *J Biol Chem* 277: 20631–
- 655 20639.
- 656 41. Zhang Y, Cho YY, Petersen BL, Zhu F, Dong Z (2004) Evidence of stat1 phosphory-
- 657 lation modulated by mapks, mek1 and msk1. *Carcinogenesis* 25: 1165–1175.
- 658 42. Li Z, Theus MH, Wei L (2006) Role of erk 1/2 signaling in neuronal differentiation of
- 659 cultured embryonic stem cells. *Dev Growth Differ* 48: 513–523.
- 660 43. Yen A, Reece SL, Albright KL (1984) Dependence of hl-60 myeloid cell differentiation
- 661 on continuous and split retinoic acid exposures: precommitment memory associated
- 662 with altered nuclear structure. *J Cell Physiol* 118: 277–286.
- 663 44. Ferrell J (2002) Self-perpetuating states in signal transduction: positive feedback,
- 664 double-negative feedback and bistability. *Curr Opin Cell Biol* 14: 140-8.
- 665 45. Xiong W, Ferrell J (2003) A positive-feedback-based bistable 'memory module' that
- 666 governs a cell fate decision. *Nature* 426: 460-5.
- 667 46. Bagci EZ, Vodovotz Y, Billiar TR, Ermentrout GB, Bahar I (2006) Bistability in apop-
- 668 tosis: roles of bax, bcl-2, and mitochondrial permeability transition pores. *Biophys J*
- 669 90: 1546-59.
- 670 47. Luan D, Zai M, Varner JD (2007) Computationally derived points of fragility of a
- 671 human cascade are consistent with current therapeutic strategies. *PLoS Comput*
- 672 *Biol* 3: e142.
- 673 48. Moon TS, Lou C, Tamsir A, Stanton BC, Voigt CA (2012) Genetic programs con-

- 700 59. Liu M, Iavarone A, Freedman LP (1996) Transcriptional activation of the human
701 p21(waf1/cip1) gene by retinoic acid receptor. correlation with retinoid induction of
702 u937 cell differentiation. J Biol Chem 271: 31723-8.
- 703 60. Bunaciu RP, Yen A (2013) 6-formylindolo (3,2-b)carbazole (ficz) enhances retinoic
704 acid (ra)-induced differentiation of hl-60 myeloblastic leukemia cells. Mol Cancer 12:
705 39.
- 706 61. Balmer JE, Blomhoff R (2002) Gene expression regulation by retinoic acid. J Lipid
707 Res 43: 1773-808.
- 708 62. Rosen ED, Hsu CH, Wang X, Sakai S, Freeman MW, et al. (2002) C/ebpalpha in-
709 duces adipogenesis through ppargamma: a unified pathway. Genes Dev 16: 22-6.
- 710 63. Varley CL, Bacon EJ, Holder JC, Southgate J (2009) Foxa1 and irf-1 intermediary
711 transcriptional regulators of ppargamma-induced urothelial cytodifferentiation. Cell
712 Death Differ 16: 103-14.
- 713 64. Bruemmer D, Yin F, Liu J, Berger JP, Sakai T, et al. (2003) Regulation of the growth
714 arrest and dna damage-inducible gene 45 (gadd45) by peroxisome proliferator-
715 activated receptor gamma in vascular smooth muscle cells. Circ Res 93: e38-47.
- 716 65. Delerive P, De Bosscher K, Besnard S, Vanden Berghe W, Peters JM, et al. (1999)
717 Peroxisome proliferator-activated receptor alpha negatively regulates the vascular
718 inflammatory gene response by negative cross-talk with transcription factors nf-
719 kappaB and ap-1. J Biol Chem 274: 32048-54.
- 720 66. Altinok S, Xu M, Spiegelman BM (1997) Ppargamma induces cell cycle withdrawal:
721 inhibition of e2f/dp dna-binding activity via down-regulation of pp2a. Genes Dev 11:
722 1987-98.
- 723 67. Fei J, Cook C, Gillespie M, Yu B, Fullen K, et al. (2011) Atherogenic ω -6 lipids mod-
724 ulate ppar- egr-1 crosstalk in vascular cells. PPAR Res 2011: 753917.
- 725 68. Song EK, Lee YR, Kim YR, Yeom JH, Yoo CH, et al. (2012) Naadp mediates insulin-

- 726 stimulated glucose uptake and insulin sensitization by ppar γ in adipocytes. Cell Rep
727 2: 1607-19.
- 728 69. Szanto A, Nagy L (2005) Retinoids potentiate peroxisome proliferator-activated re-
729 ceptor gamma action in differentiation, gene expression, and lipid metabolic pro-
730 cesses in developing myeloid cells. Mol Pharmacol 67: 1935-43.
- 731 70. Han S, Sidell N, Fisher PB, Roman J (2004) Up-regulation of p21 gene expres-
732 sion by peroxisome proliferator-activated receptor gamma in human lung carcinoma
733 cells. Clin Cancer Res 10: 1911-9.
- 734 71. Von Knethen A, Brüne B (2002) Activation of peroxisome proliferator-activated re-
735 ceptor gamma by nitric oxide in monocytes/macrophages down-regulates p47phox
736 and attenuates the respiratory burst. J Immunol 169: 2619-26.
- 737 72. Dispirito JR, Fang B, Wang F, Lazar MA (2013) Pruning of the adipocyte peroxisome
738 proliferator-activated receptor γ cistrome by hematopoietic master regulator pu.1.
739 Mol Cell Biol 33: 3354-64.
- 740 73. Chen H, Ray-Gallet D, Zhang P, Hetherington CJ, Gonzalez DA, et al. (1995) Pu.1
741 (spi-1) autoregulates its expression in myeloid cells. Oncogene 11: 1549-60.
- 742 74. Steidl U, Rosenbauer F, Verhaak RGW, Gu X, Ebralidze A, et al. (2006) Essential
743 role of jun family transcription factors in pu.1 knockdown-induced leukemic stem
744 cells. Nat Genet 38: 1269-77.
- 745 75. Laslo P, Spooner CJ, Warmflash A, Lancki DW, Lee HJ, et al. (2006) Multilineage
746 transcriptional priming and determination of alternate hematopoietic cell fates. Cell
747 126: 755-66.
- 748 76. Pahl HL, Scheibe RJ, Zhang DE, Chen HM, Galson DL, et al. (1993) The proto-
749 oncogene pu.1 regulates expression of the myeloid-specific cd11b promoter. J Biol
750 Chem 268: 5014-20.
- 751 77. Yuki H, Ueno S, Tatetsu H, Niiro H, Iino T, et al. (2013) Pu.1 is a potent tumor

- 752 suppressor in classical hodgkin lymphoma cells. Blood 121: 962-70.
- 753 78. Li SL, Schlegel W, Valente AJ, Clark RA (1999) Critical flanking sequences of pu.1
754 binding sites in myeloid-specific promoters. J Biol Chem 274: 32453-60.
- 755 79. Dahl R, Walsh JC, Lancki D, Laslo P, Iyer SR, et al. (2003) Regulation of macrophage
756 and neutrophil cell fates by the pu.1:c/ebpalpha ratio and granulocyte colony-
757 stimulating factor. Nat Immunol 4: 1029-36.
- 758 80. Timchenko N, Wilson DR, Taylor LR, Abdelsayed S, Wilde M, et al. (1995) Autoreg-
759 ulation of the human c/ebp alpha gene by stimulation of upstream stimulatory factor
760 binding. Mol Cell Biol 15: 1192-202.
- 761 81. Lidonnici MR, Audia A, Soliera AR, Prisco M, Ferrari-Amorotti G, et al. (2010) Ex-
762 pression of the transcriptional repressor gfi-1 is regulated by c/ebpalpha and is
763 involved in its proliferation and colony formation-inhibitory effects in p210bcr/abl-
764 expressing cells. Cancer Res 70: 7949-59.
- 765 82. D'Alo' F, Johansen LM, Nelson EA, Radomska HS, Evans EK, et al. (2003) The
766 amino terminal and e2f interaction domains are critical for c/ebp alpha-mediated
767 induction of granulopoietic development of hematopoietic cells. Blood 102: 3163-
768 71.
- 769 83. Pan Z, Hetherington CJ, Zhang DE (1999) Ccaat/enhancer-binding protein activates
770 the cd14 promoter and mediates transforming growth factor beta signaling in mono-
771 cyte development. J Biol Chem 274: 23242-8.
- 772 84. Harris TE, Albrecht JH, Nakanishi M, Darlington GJ (2001) Ccaat/enhancer-binding
773 protein-alpha cooperates with p21 to inhibit cyclin-dependent kinase-2 activity and
774 induces growth arrest independent of dna binding. J Biol Chem 276: 29200-9.
- 775 85. Bauvois B, Durant L, Laboureau J, Barthélémy E, Rouillard D, et al. (1999) Upreg-
776 ulation of cd38 gene expression in leukemic b cells by interferon types i and ii. J
777 Interferon Cytokine Res 19: 1059-66.

- 778 86. Passioura T, Dolnikov A, Shen S, Symonds G (2005) N-ras-induced growth suppres-
779 sion of myeloid cells is mediated by irf-1. *Cancer Res* 65: 797-804.
- 780 87. Dahl R, Iyer SR, Owens KS, Cuylear DD, Simon MC (2007) The transcriptional
781 repressor gfi-1 antagonizes pu.1 activity through protein-protein interaction. *J Biol
782 Chem* 282: 6473-83.
- 783 88. Duan Z, Horwitz M (2003) Targets of the transcriptional repressor oncoprotein gfi-1.
784 *Proc Natl Acad Sci U S A* 100: 5932-7.
- 785 89. Chen H, Zhang P, Radomska HS, Hetherington CJ, Zhang DE, et al. (1996) Octamer
786 binding factors and their coactivator can activate the murine pu.1 (spi-1) promoter.
787 *J Biol Chem* 271: 15743-52.
- 788 90. Behre G, Whitmarsh AJ, Coghlan MP, Hoang T, Carpenter CL, et al. (1999) c-jun
789 is a jnk-independent coactivator of the pu.1 transcription factor. *J Biol Chem* 274:
790 4939-46.
- 791 91. Kardassis D, Papakosta P, Pardali K, Moustakas A (1999) c-jun transactivates the
792 promoter of the human p21(waf1/cip1) gene by acting as a superactivator of the
793 ubiquitous transcription factor sp1. *J Biol Chem* 274: 29572-81.
- 794 92. Johnson DG, Ohtani K, Nevins JR (1994) Autoregulatory control of e2f1 expression
795 in response to positive and negative regulators of cell cycle progression. *Genes Dev*
796 8: 1514-25.
- 797 93. Fu M, Zhang J, Lin Y, Zhu X, Ehrengruber MU, et al. (2002) Early growth response
798 factor-1 is a critical transcriptional mediator of peroxisome proliferator-activated
799 receptor-gamma 1 gene expression in human aortic smooth muscle cells. *J Biol
800 Chem* 277: 26808-14.
- 801 94. Mak KS, Funnell APW, Pearson RCM, Crossley M (2011) Pu.1 and haematopoietic
802 cell fate: Dosage matters. *Int J Cell Biol* 2011: 808524.
- 803 95. Chen F, Wang Q, Wang X, Studzinski GP (2004) Up-regulation of egr1 by 1,25-

- 804 dihydroxyvitamin d3 contributes to increased expression of p35 activator of cyclin-
805 dependent kinase 5 and consequent onset of the terminal phase of hl60 cell differ-
806 entiation. *Cancer Res* 64: 5425-33.
- 807 96. Suh J, Jeon YJ, Kim HM, Kang JS, Kaminski NE, et al. (2002) Aryl hydrocarbon
808 receptor-dependent inhibition of ap-1 activity by 2,3,7,8-tetrachlorodibenzo-p-dioxin
809 in activated b cells. *Toxicol Appl Pharmacol* 181: 116-23.
- 810 97. Shen M, Bunaciu RP, Congleton J, Jensen HA, Sayam LG, et al. (2011) Inter-
811 feron regulatory factor-1 binds c-cbl, enhances mitogen activated protein kinase
812 signaling and promotes retinoic acid-induced differentiation of hl-60 human myelo-
813 monoblastic leukemia cells. *Leuk Lymphoma* 52: 2372-9.
- 814 98. Bunaciu RP, Yen A (2011) Activation of the aryl hydrocarbon receptor ahr promotes
815 retinoic acid-induced differentiation of myeloblastic leukemia cells by restricting ex-
816 pression of the stem cell transcription factor oct4. *Cancer Res* 71: 2371-80.
- 817 99. Jackson DA, Pombo A, Iborra F (2000) The balance sheet for transcription: an anal-
818 ysis of nuclear rna metabolism in mammalian cells. *FASEB J* 14: 242-54.
- 819 100. Zhao ZW, Roy R, Gebhardt JCM, Suter DM, Chapman AR, et al. (2014) Spatial orga-
820 nization of rna polymerase ii inside a mammalian cell nucleus revealed by reflected
821 light-sheet superresolution microscopy. *Proc Natl Acad Sci U S A* 111: 681-6.
- 822 101. Freitas R, Merkle R (2004) Kinematic Self-Replicating Machines. Oxford University
823 Press.
- 824 102. Yang E, van Nimwegen E, Zavolan M, Rajewsky N, Schroeder M, et al. (2003) De-
825 cay rates of human mrnas: correlation with functional characteristics and sequence
826 attributes. *Genome Res* 13: 1863-72.
- 827 103. Doherty MK, Hammond DE, Clague MJ, Gaskell SJ, Beynon RJ (2009) Turnover
828 of the human proteome: determination of protein intracellular stability by dynamic
829 silac. *J Proteome Res* 8: 104-12.

- 830 104. Darzacq X, Shav-Tal Y, de Turris V, Brody Y, Shenoy SM, et al. (2007) In vivo dy-
831 namics of rna polymerase ii transcription. Nat Struct Mol Biol 14: 796-806.
- 832 105. Boström K, Wettsten M, Borén J, Bondjers G, Wiklund O, et al. (1986) Pulse-chase
833 studies of the synthesis and intracellular transport of apolipoprotein b-100 in hep g2
834 cells. J Biol Chem 261: 13800-6.
- 835 106. Meyers R, editor (2004) Encyclopedia of Molecular Cell Biology and Molecular
836 Medicine, Volume 1, 2nd Edition. ISBN: 978-3-527-30543-8. Wiley-Blackwell.
- 837 107. Rosenbluth MJ, Lam WA, Fletcher DA (2006) Force microscopy of nonadherent
838 cells: a comparison of leukemia cell deformability. Biophys J 90: 2994-3003.

Table 1: Myelomonocytic transcription factor connectivity used in the signal integration and phenotype modules.

839

840

| Effector | Effect | Target | Source |
|----------------|--------|----------------|--------|
| RAR α | + | RAR α | (53) |
| | + | PU.1 | (54) |
| | + | C/EBP α | (55) |
| | + | IRF-1 | (56) |
| | - | Oct4 | (57) |
| | + | CD38 | (58) |
| | + | p21 | (59) |
| | + | AhR | (60) |
| | + | EGR1 | (61) |
| PPAR γ | + | C/EBP α | (62) |
| | + | IRF-1 | (63) |
| | + | Oct1 | (64) |
| | - | AP-1 | (65) |
| | - | E2F | (66) |
| | - | EGR1 | (67) |
| | + | CD38 | (68) |
| | + | CD14 | (69) |
| | + | p21 | (70) |
| | - | p47phox | (71) |
| PU.1 | - | PPAR γ | (72) |
| | + | PU.1 | (73) |
| | + | AP-1 | (74) |
| | + | EGR1 | (75) |
| | + | CD11b | (76) |
| | + | p21 | (77) |
| | + | p47phox | (78) |
| C/EBP α | + | PPAR γ | (62) |
| | + | PU.1 | (79) |
| | + | C/EBP α | (80) |
| | + | Gfi-1 | (81) |
| | - | E2F | (82) |
| | + | CD14 | (83) |

| | | | |
|-------|---|----------------|------|
| | + | p21 | (84) |
| IRF-1 | + | CD38 | (85) |
| | + | p21 | (86) |
| | - | PU.1 | (87) |
| | - | C/EBP α | (88) |
| | - | E2F | (88) |
| | - | EGR1 | (75) |
| | - | p21 | (88) |
| Oct1 | + | PU.1 | (89) |
| AP-1 | - | PPAR γ | (65) |
| | + | PU.1 | (90) |
| | + | p21 | (91) |
| E2F | + | E2F | (92) |
| EGR1 | + | PPAR γ | (93) |
| | - | Gfi-1 | (94) |
| | + | CD14 | (95) |
| AhR | + | AP-1 | (96) |
| | + | IRF-1 | (97) |
| | - | Oct4 | (98) |
| | - | PU.1 | |

Table 2: Characteristic model parameters estimated from literature.

| Symbol | Description | Value | Units | Source | |
|----------------|--|---------------------|---------------|------------|------------|
| R_1 | RNA polymerase abundance | 75,000 | copies/cell | (99, 100) | |
| R_2 | Ribosome abundance | 1×10^6 | copies/cell | (101) | |
| G_i | Characteristic gene abundance | 2 | copies/cell | this study | |
| K_X | Saturation constant transcription | 4,600 | copies/cell | this study | |
| K_T | Saturation constant translation | 100,000 | copies/cell | this study | |
| $t_{1/2,m}$ | characteristic mRNA half-life (transcription factor) | 2 | hr | (102) | |
| $t_{1/2,p}$ | characteristic protein half-life | 10 | hr | (103) | |
| $\theta_{m,j}$ | characteristic mRNA degradation constant | 0.34 | hr^{-1} | derived | |
| $\theta_{p,j}$ | characteristic protein degradation constant | 0.07 | hr^{-1} | derived | |
| 843 | t_d | HL-60 doubling time | 19.5 | hr | this study |
| | μ | growth rate | 0.035 | hr^{-1} | derived |
| | k_d | death rate | 0.10μ | hr^{-1} | derived |
| e_T | elongation rate RNA polymerase | 6 | nt/s | (104) | |
| e_X | elongation rate Ribosome | 5 | aa/s | (105) | |
| $L_{T,o}$ | characteristic gene length | 15,000 | nt | (106) | |
| $L_{X,o}$ | characteristic transcript length | 5,000 | nt | derived | |
| k_T | characteristic transcription rate | 1.44 | hr^{-1} | derived | |
| k_X | characteristic translation rate | 3.60 | hr^{-1} | derived | |
| D | Diameter of an HL-60 cell | 12.4 | μm^3 | (107) | |
| f_C | cytoplasmic fraction | 0.51 | dimensionless | (107) | |

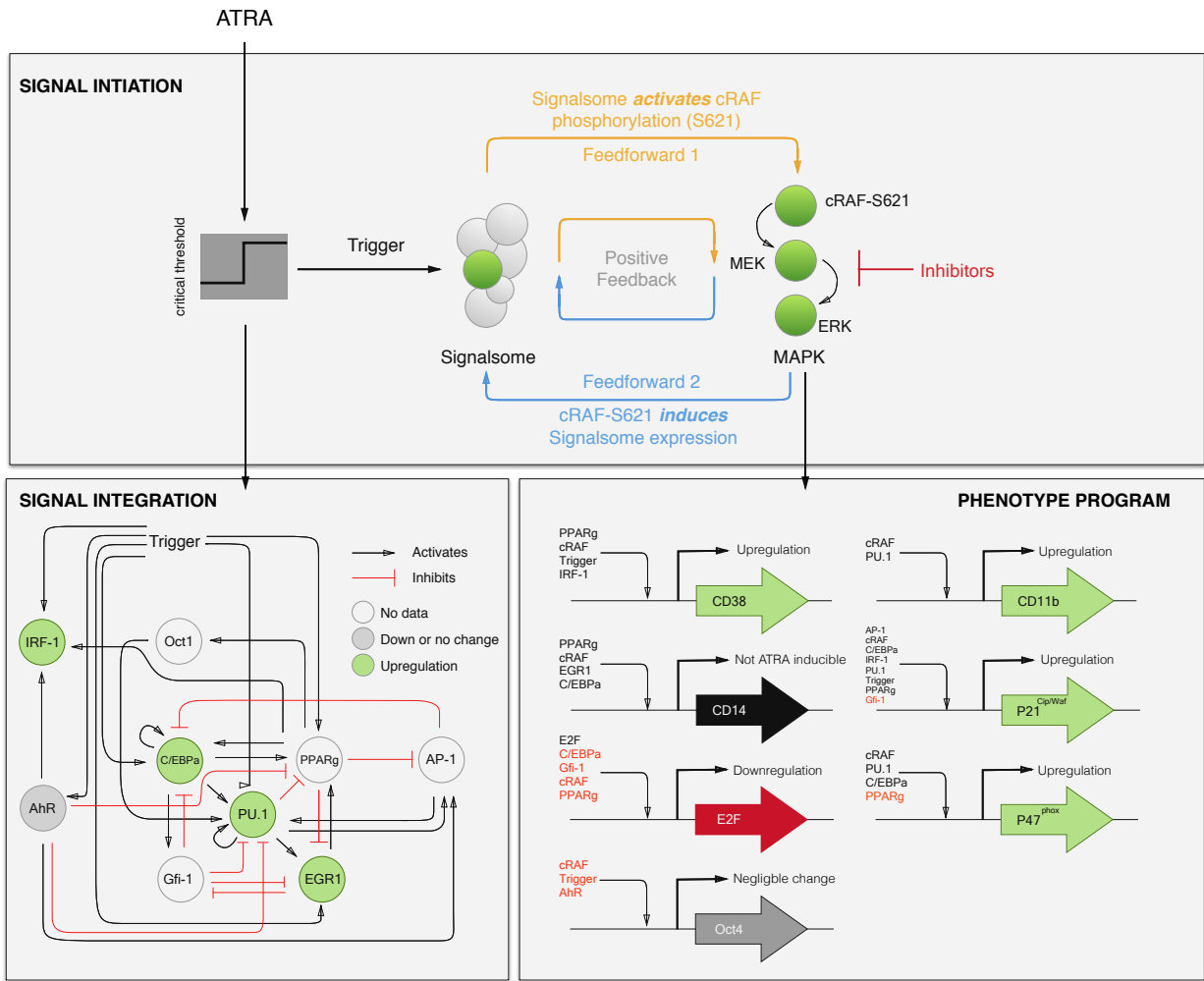


Fig. 1: Schematic of the effective ATRA differentiation circuit. Above a critical threshold, ATRA activates an upstream Trigger, which induces signalsome complex formation. Signalsome activates the mitogen-activated protein kinase (MAPK) cascade which in turn drives the differentiation program and signalsome formation. Both Trigger and activated cRaf-pS621 drive a phenotype gene expression program responsible for differentiation. Trigger activates the expression of a series of transcription factors which in combination with cRaf-pS621 result in phenotypic change.

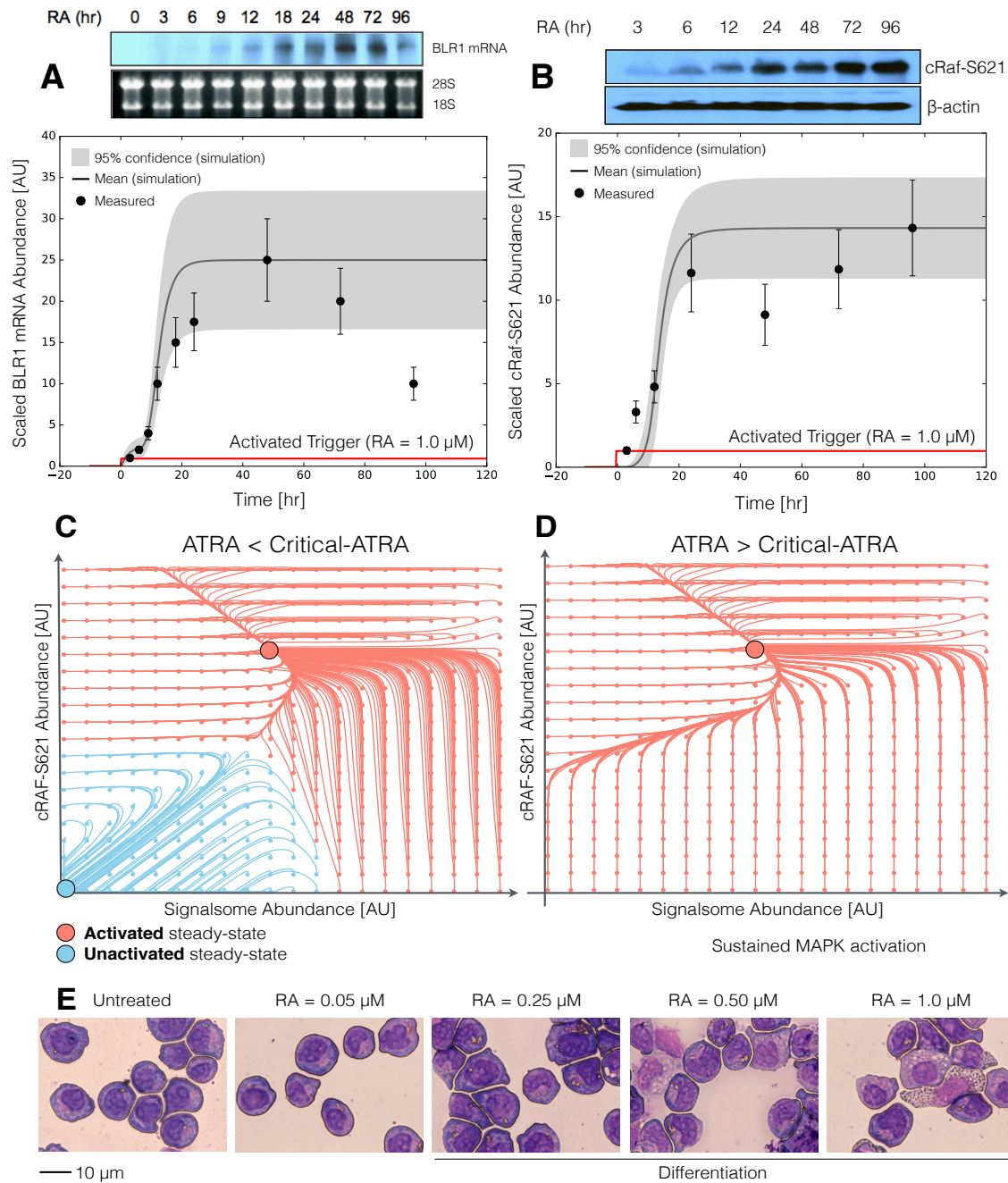


Fig. 2: Model analysis for ATRA-induced HL-60 differentiation. A: BLR1 mRNA versus time following exposure to 1 μ M ATRA at t = 0 hr. B: cRaf-pS621 versus time following exposure to 1 μ M ATRA at t = 0 hr. Points denote experimental measurements, solid lines denote the mean model performance. Shaded regions denote the 99% confidence interval calculated over the parameter ensemble. C: Signalsome and cRaf-pS621 nullclines for ATRA below the critical threshold. The model had two stable steady states and a single unstable state in this regime. D: Signalsome and cRaf-pS621 nullclines for ATRA above the critical threshold. In this regime the model had only a single stable steady state. E: Morphology of HL-60 as a function of ATRA concentration (t = 72 hr).

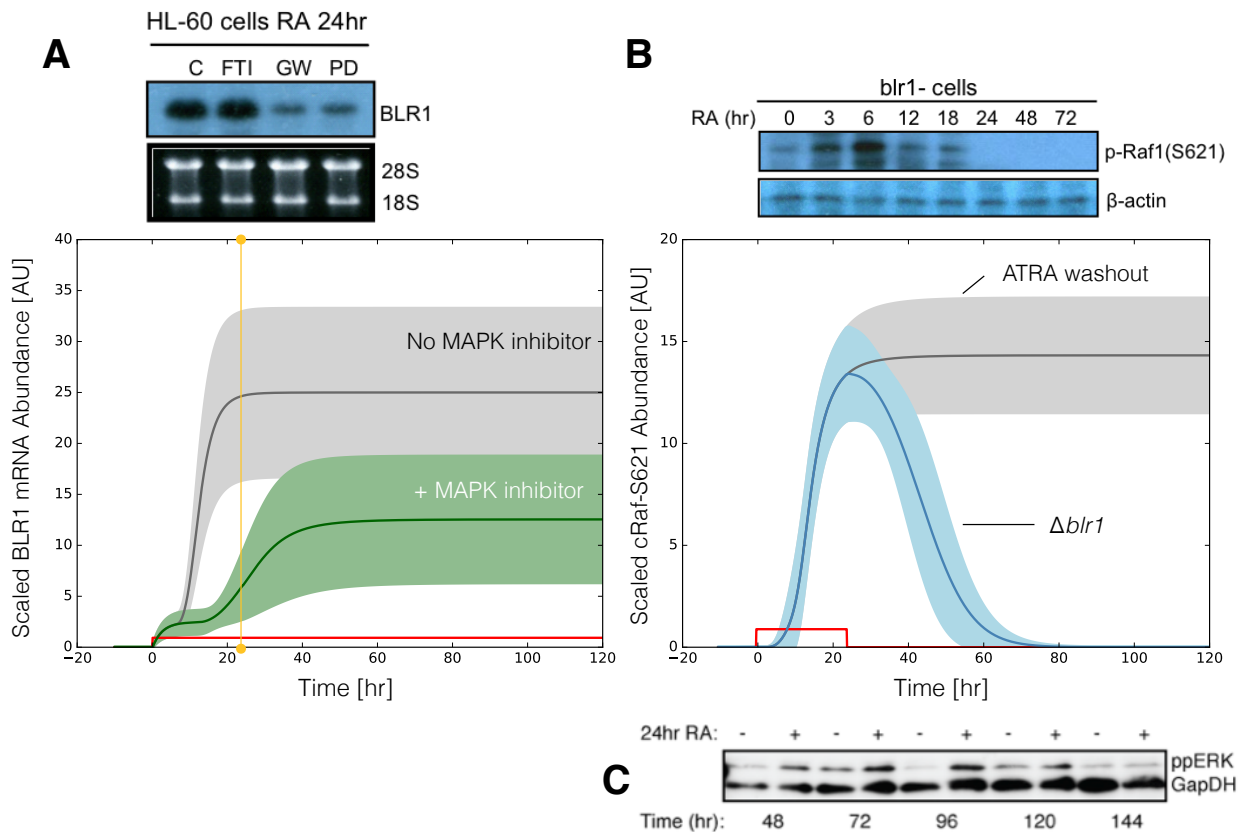


Fig. 3: Model simulation following exposure to $1\mu\text{M}$ ATRA. A: BLR1 mRNA versus time with and without MAPK inhibitor. B: cRaf-pS621 versus time following pulsed exposure to $1\mu\text{M}$ ATRA with and without BLR1. Solid lines denote the mean model performance, while shaded regions denote the 99% confidence interval calculated over the parameter ensemble. C: Western blot analysis of phosphorylated ERK1/2 in ATRA washout experiments. Experimental data in panels A and B were reproduced from Wang and Yen (20), data in panel C is reported in this study.

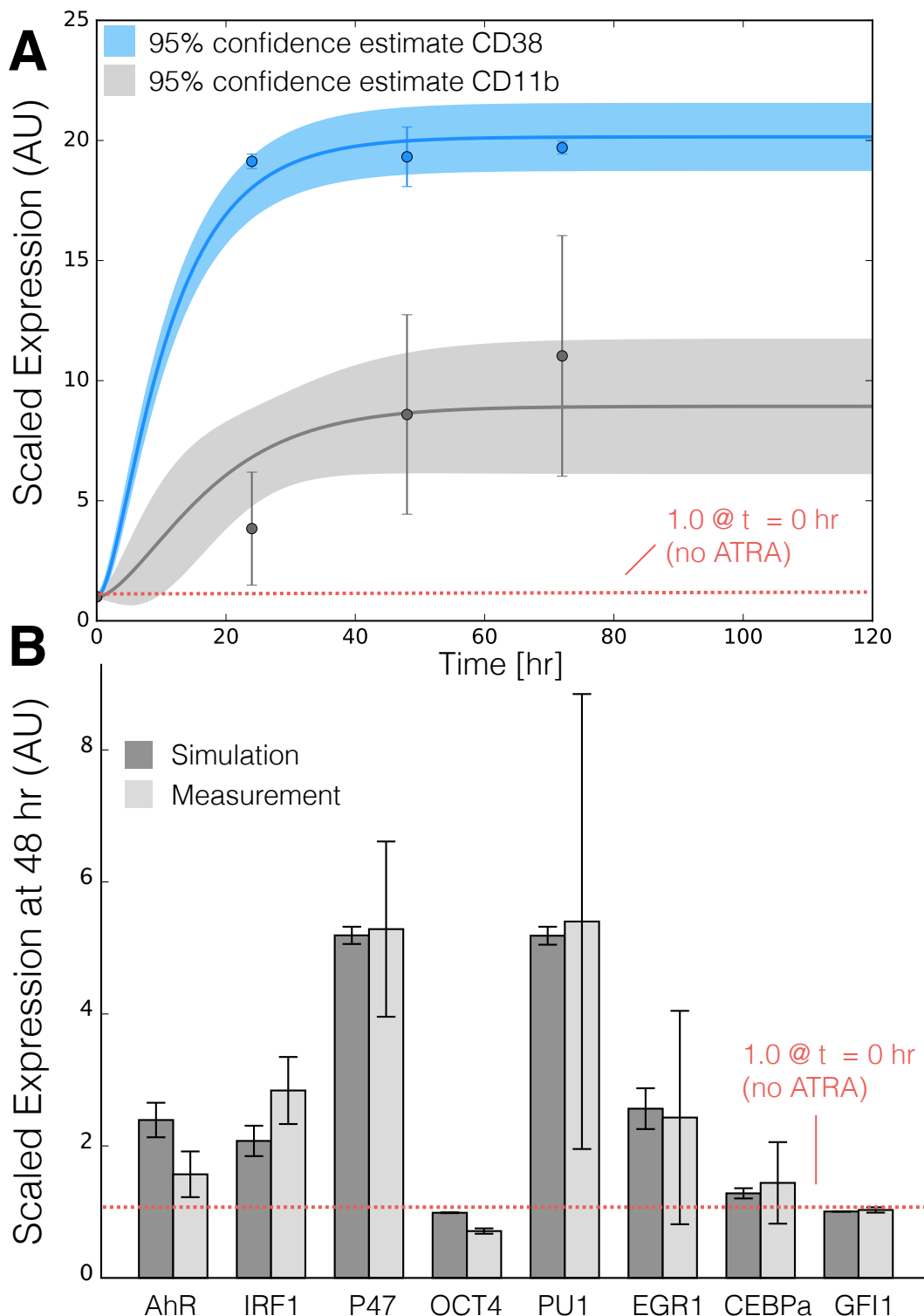


Fig. 4: Model simulation of the HL-60 gene expression program following exposure to $1\mu\text{M}$ ATRA at $t = 0$ hr. A: CD38 and CD11b expression versus time following ATRA exposure at time $t = 0$ hr. B: Gene expression at $t = 48$ hr following ATRA exposure. Experimental data in panels A and B were reproduced from Jensen et al. (25).

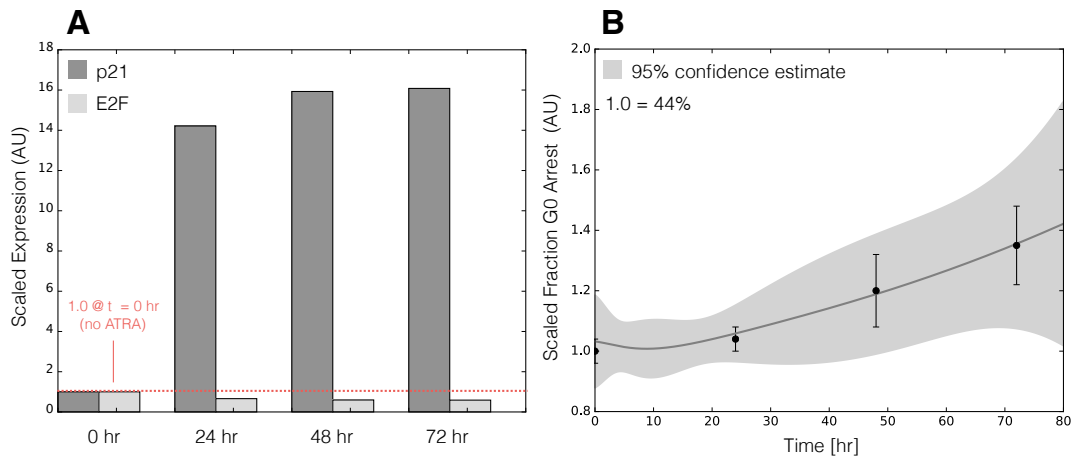


Fig. 5: Model simulation of HL-60 cell-cycle arrest following exposure to $1\mu\text{M}$ ATRA at $t = 0$ hr. A: Predicted P21 and E2F expression levels for the best parameter set following ATRA exposure at time $t = 0$ hr. B: Estimated fraction of HL-60 cells in G0 arrest following ATRA exposure at time $t = 0$ hr. The gray region denotes the 95% confidence estimate of the polynomial model. Experimental data in panel B was reproduced from Jensen et al. (25).

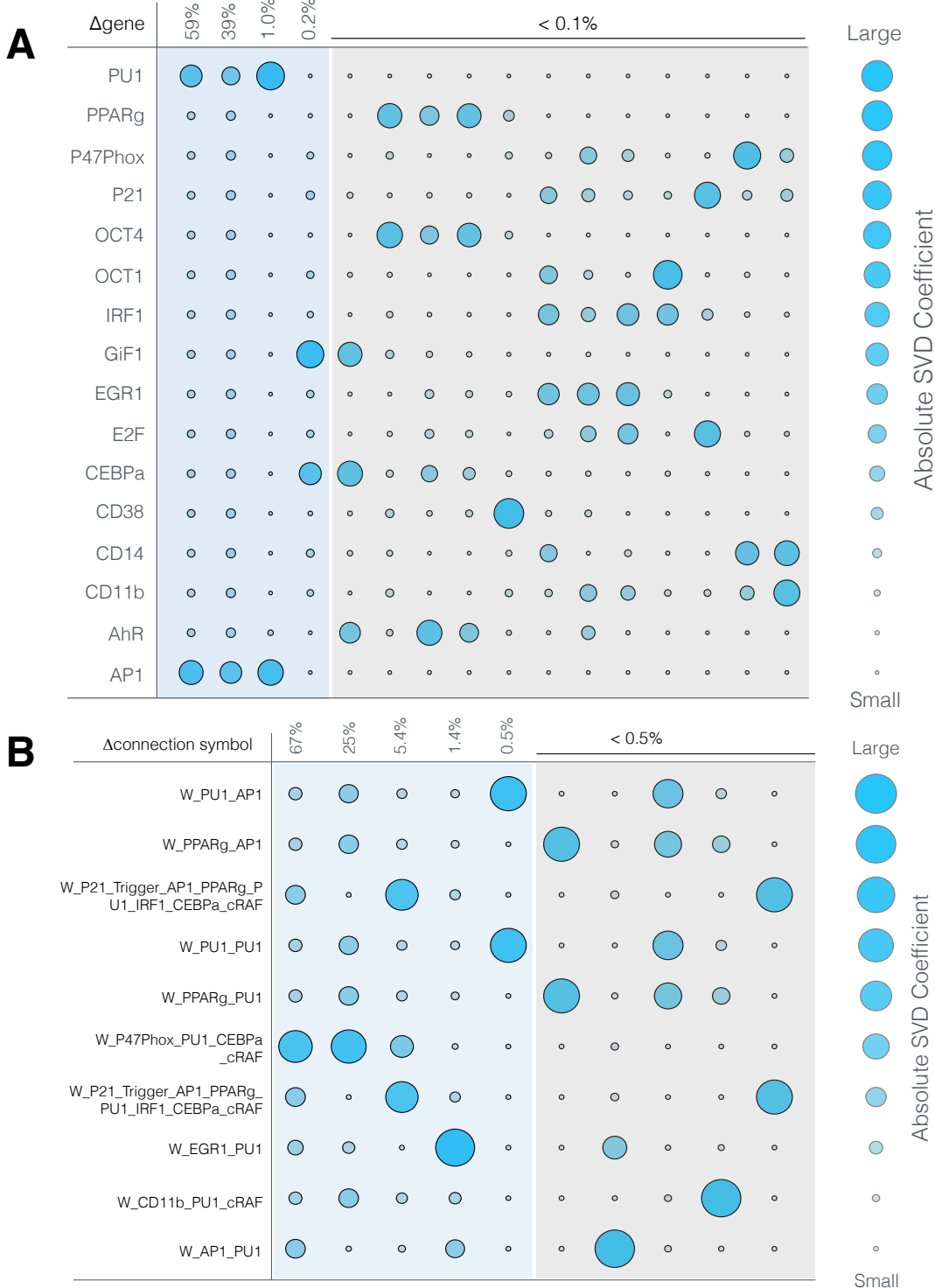


Fig. 6: Robustness of the HL-60 differentiation program following exposure to $1\mu\text{M}$ ATRA at $t = 0$ hr. A: Singular value decomposition of the system response (l^2 -norm between the perturbed and nominal state) following pairwise gene knockout simulations using the best fit parameter set. The percentage at the top of each column describes the fraction of the variance in the system state captured by the node combinations in the rows. B: Singular value decomposition of the system response (l^2 -norm between the perturbed and nominal state) following the pairwise removal of connections from the PU.1 and AP1 nodes.

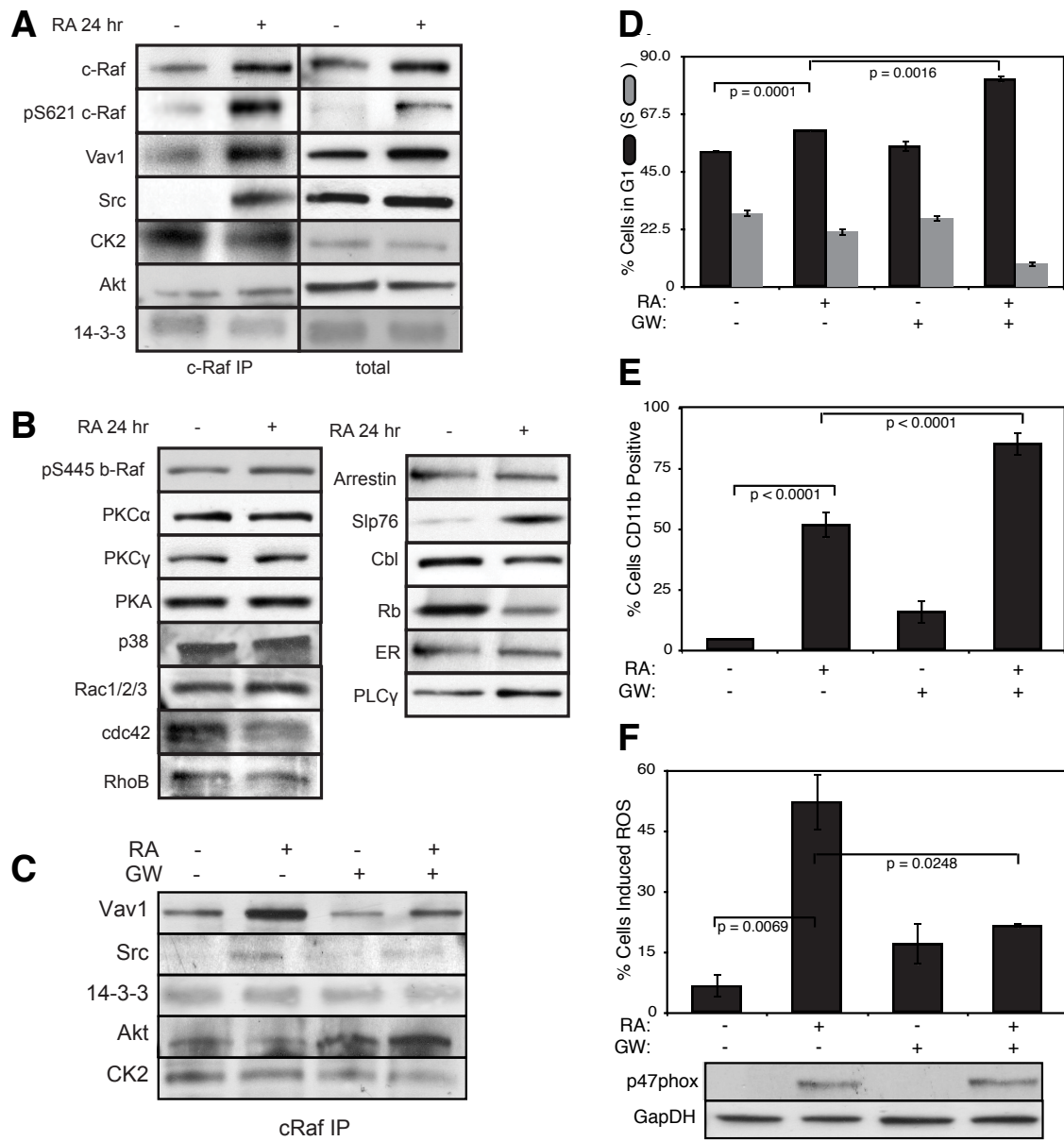


Fig. 7: Investigation of a panel of possible Raf interaction partners in the presence and absence of ATRA. A: Species identified to precipitate out with Raf: first column shows Western blot analysis on total Raf immunoprecipitation with and without 24 hr ATRA treatment and the second on total lysate. B: The expression of species considered that did not precipitate out with Raf at levels detectable by Western blot analysis on total lysate. C: Effect of the Raf inhibitor GW5074 on Raf interactions as determined by Western blot analysis of total Raf immunoprecipitation. The Authors note the signal associated with Src was found to be weak. D: Cell Cycle distribution as determined by flow cytometry indicated arrest induced by ATRA, which was increased by the addition of GW5074. E: Expression of the cell surface marker CD11b as determined by flow cytometry indicated increased expression induced by ATRA, which was enhanced by the addition of GW5074. F: Inducible reactive oxygen species (ROS) as determined by DCF flow cytometry. The functional differentiation response of ATRA treated cells was mitigated by GW5074.